Interplay of topology and geometry in frustrated two-dimensional Heisenberg magnets

N. Hasselmann[1] and A. Sinner[2]
[1]*Max-Planck-Institute for Solid State Research, Heisenbergstrasse 1, D-70569 Stuttgart, Germany*
[2]*Institut für Physik, Universität Augsburg, D-86135 Augsburg, Germany*
(Received 23 October 2013; revised manuscript received 18 August 2014; published 4 September 2014)

We investigate two-dimensional frustrated Heisenberg magnets using nonperturbative renormalization group techniques. These magnets allow for pointlike topological defects which are believed to unbind and drive either a crossover or a phase transition which separates a low-temperature, spin-wave-dominated regime from a high-temperature regime where defects are abundant. Our approach can account for the crossover qualitatively and both the temperature dependence of the correlation length as well as a broad but well-defined peak in the specific heat are reproduced. We find no signatures of a finite-temperature transition and an accompanying diverging length scale. Our analysis is consistent with a rapid crossover driven by topological defects.

DOI: 10.1103/PhysRevB.90.094404 PACS number(s): 75.10.Hk, 64.60.ae, 11.10.Hi

I. INTRODUCTION

Frustrated magnets have a number of highly fascinating properties which have been the focus of intense research interest for some time. These include magnets which do not order but where a macroscopic number of competing low-lying states give rise to strong correlations and a large low-temperature entropy or spin liquids where quantum fluctuations prevent ordering and exotic quasiparticles appear; see Ref. [1] for a recent review. A much simpler situation arises in classical magnets if the frustration is not sufficiently strong to prevent an ordered ground state. In this case the ground state has a broken symmetry and the low-temperature excitations are just spin waves. However, even classical frustrated magnets which do order are not completely understood, which can be attributed in large part to a nontrivial order parameter which characterizes such magnets. In $d = 2$, as was first pointed out by Kawamura and Miyashita [2], the order parameter manifold of a frustrated Heisenberg magnet allows for pointlike topological Z_2 defects and the influence of these defects on the properties of the magnet at finite temperatures proved very difficult to quantify. In two-dimensional collinear XY magnets topological defects are responsible for the Berezinskii-Kosterlitz-Thouless (BKT) transition. However, in this case the perturbative β function of the XY coupling constant, which is sensitive only to the geometry but not the topology of the order parameter space, vanishes. This is very different from the situation in frustrated Heisenberg magnets.

The major difficulty with two-dimensional frustrated Heisenberg magnets is the combined presence of both pointlike defects, originating from the topological properties of the order parameter space [2], and the phenomenon of asymptotic freedom which has its root in the local geometry of the order parameter space. In contrast to collinear XY magnets, where the Villain approximation makes it possible to map the problem on the two-dimensional Coulomb gas, which can be well studied using renormalization group (RG) techniques [3], no similar tool is available for frustrated Heisenberg models. The yet-unsolved question is whether a finite-temperature transition exists in frustrated Heisenberg magnets. In particular, for the simplest such model, the Heisenberg antiferromagnet on a triangular lattice (HAFT), this question has been addressed repeatedly over the years, without a definite conclusion. Monte Carlo (MC) simulations of the HAFT have found indications of a vortex unbinding at a finite temperature T_{cross} [4–6]. The vorticity modulus, which measures the response of the magnet to an imposed twist along a path which encloses a vortex core, has been shown to vanish [4] at T_{cross}. Further indications of a finite-temperature transition can be found from the phase diagram of the HAFT in a magnetic field [7,8]. In small fields, there are two finite-temperature transitions. There is a BKT transition from a low-temperature canted state with quasi-long-range order of the transverse spin components to an intermediate state which has a vanishing spin stiffness. A second transition at higher temperatures restores the sublattice symmetry of the magnet, which is broken in both low-temperature phases. It is unclear from MC what happens in the zero-field limit, but both transitions are of the order of $T_c \approx 0.3J$ (where J is antiferromagnetic exchange constant) for very small fields, a similar temperature to where at zero field a vortex unbinding seems to occur. In a perturbative RG analysis some indication of a fixed point in $d = 2$ which might correspond to a topological phase transition was reported [9]; see, however, also Ref. [10]. Experimentally, there are also several reports on indications of a vortex-driven transition [11–14].

Perhaps the cleanest demonstration of the role of topology comes from a comparison of MC simulations of two different matrix models representing interacting tops, which both share the same geometrical properties but differ in their topology [15]. The model which allows for topological defects shows a clear finite-temperature peak in the specific heat and a crossover in the correlation length dependence on T which are both absent in the topological trivial model.

The properties of the long wavelength modes of the magnet are described by a nonlinear σ model (NLσM). The order parameter space for a frustrated Heisenberg magnet has the symmetry $SO(3) \times SO(2)/SO(2) \sim SO(3)$; see, e.g., Ref. [16,17] for a discussion of the symmetries. While this model describes well the physics of the Heisenberg antiferromagnet (AF) on the triangular lattice at low temperatures [5,18], its perturbative β function is not sensitive to the topological properties of $SO(3)$, which has a nontrivial homotopy group [2] $\pi_1[SO(3)] = Z_2$ and thus allows for topological defects which could be generated either through temperature or disorder [19].

An alternative continuum model for frustrated magnets is based on a Landau-Ginzburg action which includes also massive excitations. The advantage of using a Landau-Ginzburg model in conjunction with a nonperturbative RG (NPRG) approach is its ability to describe the BKT transition of the two-dimensional XY model, without relying on a mapping to the Coulomb gas [20]. Although it is not well understood how exactly topology enters the NPRG flow, its success in the study of the XY model makes the NPRG a promising approach to the physics of Z_2 defects in frustrated Heisenberg models. Here we follow this ansatz and present results for $d = 2$.

In Sec. II we discuss the different field theoretical approaches to the HAFT and present the Landau-Ginzburg model which we investigate here. Although the Landau-Ginzburg model applies to noncollinear ordered magnets in general, we concentrate here on the HAFT model in our numerical analysis and estimate appropriate initial values for the NPRG in Sec. II. The NPRG approach is presented in Sec. III, and the approximation of the effective average action are presented and discussed in Secs. III A and III B. The derivation of the flow equations is discussed in Sec. III C. Results for the NPRG approximation of the HAFT model are presented in Sec. IV, where we calculate both the temperature dependence of the spin correlation length and the specific heat. Our results show a clear crossover behavior of the temperature dependence of the correlation length, from a low-temperature exponential dependence characteristic as it is also obtained within a NLσM approach, to a much weaker temperature dependence at higher temperatures. This crossover is also visible as a broad but well defined peak at the crossover temperature in the specific heat. We stress that while this crossover has been repeatedly observed in MC data, it is not captured by the NLσM and it also has not yet been successfully described by other analytical approaches. We close with a summary in Sec. V.

II. THE ANTIFERROMAGNETIC HEISENBERG MODEL ON THE TRIANGULAR LATTICE

We concentrate on one of the simplest frustrated Heisenberg models, the HAFT. It is defined by

$$\mathcal{H} = J \sum_{\langle i,j \rangle} \mathbf{S}_i \cdot \mathbf{S}_j, \tag{2.1}$$

where the sum is over nearest neighbors of the triangular lattice, $\mathbf{S}_i$ are three-component unit vectors with $\mathbf{S}_i^2 = 1$, and $J > 0$. The zero-temperature ground state is the well-known planar 120° state, where neighboring spins have angles $\pm 120°$.

MC simulations [18] have convincingly demonstrated that at low temperatures the two-dimensional HAFT model is well described by a NLσM, which has the form

$$S = \frac{1}{2} \int_x \sum_{i=1}^{3} p_i (\partial_\mu \boldsymbol{n}_i)^2, \tag{2.2}$$

where the $\boldsymbol{n}_i$ are orthonormal three-component unit vectors, the p_i's are three stiffnesses (divided by the temperature), and $\int_x = \int d^d x$. Because of the planar spin orientation in the ground state one has $p_1 = p_2$, which holds both at the bare level but also throughout the renormalization group flow.

The alternative Landau-Ginzburg approach for frustrated magnets was developed early on; see, e.g., Ref. [21], and has usually been applied to study frustrated magnets close to $d = 4$. It has also been the basis of a thorough nonperturbative RG (NPRG) analysis [16,22], where flow equations were derived for all $2 < d < 4$. The central functional in the NPRG approach is the effective average action which is also the generating functional of one-particle irreducible correlation functions, and the NPRG provides a framework in which the flow of this functional connects the bare effective average action, which is identical to the bare action, to the fully renormalized generating functional of irreducible vertices [23,24]. The simplest approximation for the effective average action used in the study of frustrated magnets has the form [16,22]

$$\begin{aligned}\Gamma_\Lambda[\boldsymbol{\Phi}_1, \boldsymbol{\Phi}_2] = \int_x \Big\{ & \frac{Z_\Lambda}{2} [(\partial_\mu \boldsymbol{\Phi}_1)^2 + (\partial_\mu \boldsymbol{\Phi}_2)^2] \\ & + \frac{\lambda_\Lambda^0}{4} [\rho/2 - \kappa_\Lambda]^2 + \frac{\mu_\Lambda^0}{4} \tau \\ & + \frac{\Omega_\Lambda}{4} (\boldsymbol{\Phi}_1 \cdot \partial_\mu \boldsymbol{\Phi}_2 - \boldsymbol{\Phi}_2 \cdot \partial_\mu \boldsymbol{\Phi}_1)^2 \Big\},\end{aligned} \tag{2.3}$$

where $\rho = \mathrm{Tr}^t \Phi \Phi$ and $\tau = (1/2)\mathrm{Tr}[^t \Phi \Phi - \mathbb{1}\rho/2]^2$ are local invariants of the theory. Here the symmetry $SO(3) \times SO(2)$ for Heisenberg ($N = 3$) models has been generalized for general $N \geqslant 2$ to a $O(N) \times O(2)$ symmetry and the symmetry of the symmetry-broken ground state is $O(N-2) \times O(2)$. The subscript Λ in Γ_Λ indicates that all parameters entering (2.3) depend on the cutoff scale Λ. The fields $\boldsymbol{\Phi}_{1,2}$ have N components (the same number of components as the lattice spins), are orthogonal in the ground state, and span the planar order of a frustrated magnet [16], such as, e.g., the 120° state of the HAFT. Further, $\Phi = (\boldsymbol{\Phi}_1, \boldsymbol{\Phi}_2)$ is a $2 \times N$ matrix such that

$$^t \Phi \Phi = \begin{pmatrix} \boldsymbol{\Phi}_1 \cdot \boldsymbol{\Phi}_1 & \boldsymbol{\Phi}_1 \cdot \boldsymbol{\Phi}_2 \\ \boldsymbol{\Phi}_2 \cdot \boldsymbol{\Phi}_1 & \boldsymbol{\Phi}_2 \cdot \boldsymbol{\Phi}_2 \end{pmatrix}. \tag{2.4}$$

Thus, one has the expressions $\rho = \boldsymbol{\Phi}_1^2 + \boldsymbol{\Phi}_2^2$ and $\tau = (\boldsymbol{\Phi}_1^2 - \boldsymbol{\Phi}_2^2)^2/4 + (\boldsymbol{\Phi}_1 \cdot \boldsymbol{\Phi}_2)^2$. Both λ_Λ^0 and μ_Λ^0 are positive coupling parameters, where λ_Λ^0 controls the magnitude of the vector fields and μ_Λ^0 ensures that $\boldsymbol{\Phi}_1$ and $\boldsymbol{\Phi}_2$ are orthogonal in the ground state. If both λ_Λ^0 and μ_Λ^0 become very large, $\boldsymbol{\Phi}_1$ and $\boldsymbol{\Phi}_2$ are forced into a configuration where they are orthogonal with fixed length and, for $N = 3$, can be identified with the $\boldsymbol{n}_1$ and $\boldsymbol{n}_2$ fields of the NLSM, after a suitable rescaling such that both $\boldsymbol{\Phi}_1$, $\boldsymbol{\Phi}_2$ have norm one. The third field $\boldsymbol{n}_3$ of the NLσM is not independent of $\boldsymbol{n}_1$ and $\boldsymbol{n}_2$ but fixed by the relation $\boldsymbol{n}_3 = \boldsymbol{n}_1 \times \boldsymbol{n}_2$. However, to recover correctly the three independent fluctuation terms $(\partial_\mu \boldsymbol{n}_i)^2$ of the $\boldsymbol{n}_i$ fields within the Ginzburg-Landau model (2.3), it is necessary to add the Ω_Λ-derivative term, which is the only derivative term at fourth order in the fields, which directly renormalizes the gapless modes of the model [16,22,25].

A central role is played by the parameter κ_Λ, which is the order parameter of the theory. It gives the magnitude of the ordered magnetization (the canted 120° magnetization) around which ρ, which corresponds to the local magnetization, fluctuates. It is initially finite, since the IR modes are cut off, but the further the IR cutoff Λ is reduced, the stronger

κ_Λ is suppressed (for $d = 2$). The vanishing of κ_Λ at some finite scale Λ signals the absence of 120° order and the spin-correlation length is then determined by $2\pi/\Lambda$.

For the case considered here, the triangular AF, we have $N = 3$ and the fields $\mathbf{\Phi}_{1,2}$ can be locally related to the microscopic spins of the triangular AF. This is done by partitioning the spins first into plaquettes of three spins, where each of the spins belongs to one of the three sublattices associated with a 120° order. We then have [26]

$$\frac{3}{\sqrt{2}}\mathbf{\Phi}_1 = -\frac{1}{2}(\sqrt{3}+1)\boldsymbol{S}_1 + \frac{1}{2}(\sqrt{3}-1)\boldsymbol{S}_2 + \boldsymbol{S}_3\,, \quad (2.5a)$$

$$\frac{3}{\sqrt{2}}\mathbf{\Phi}_2 = \frac{1}{2}(\sqrt{3}-1)\boldsymbol{S}_1 - \frac{1}{2}(\sqrt{3}+1)\boldsymbol{S}_2 + \boldsymbol{S}_3\,, \quad (2.5b)$$

where $\boldsymbol{S}_1, \ldots, \boldsymbol{S}_3$ are the three spins of a local triangular plaquette. Note that we have for three spins six degrees of freedom, the same number as we have in the two unconstrained three-component fields $\mathbf{\Phi}_1$ and $\mathbf{\Phi}_2$. One can easily check that $\mathbf{\Phi}_1 \cdot \mathbf{\Phi}_2 = (2/9)(2\boldsymbol{S}_1 \cdot \boldsymbol{S}_2 - \boldsymbol{S}_1 \cdot \boldsymbol{S}_3 - \boldsymbol{S}_2 \cdot \boldsymbol{S}_3)$ and $(\boldsymbol{S}_1 + \boldsymbol{S}_2 + \boldsymbol{S}_3)^2 = 9(1 - \mathbf{\Phi}_1^2/2 - \mathbf{\Phi}_2^2/2)$, which both vanish in the perfectly ordered 120° ground state in which the fields are chosen to be normalized such that $\mathbf{\Phi}_{1,2}^2 = 1$. As we discuss in more detail below, the model defined by Eq. (2.3) supports $2N$ modes of which $2N - 3$ are gapless at $T = 0$. There are two modes with gaps $\kappa_\Lambda \mu_\Lambda^0$ and one with a mass $\kappa_\Lambda \lambda_\Lambda^0$. At any finite temperature all modes eventually become gapped; however, at very small temperatures the IR physics is completely dominated by the $2N - 3$ modes which are initially gapless. This low-temperature regime is well described by a NLσM. In principle, it would also be possible to start our investigation from the paramagnetic phase, which has $\kappa = 0$; however, it is then far more difficult to ensure that the symmetries of the model are not violated in the flow. Thus, within the same spirit as in the NLσM approach, we assume a local order and investigate how this order is destroyed by fluctuations.

The relation between the NLσM and the NPRG approach near $d = 2$ (and for any N) has been established in Ref. [16] who showed that in the limit of large masses the NPRG reduces to

$$\partial_\ell \eta_1 = -(d-2)\eta_1 + N - 2 - \frac{\eta_2}{2\eta_1}\,, \quad (2.6a)$$

$$\partial_\ell \eta_2 = -(d-2)\eta_2 + \frac{N-2}{2}\left(\frac{\eta_2}{\eta_1}\right)^2\,, \quad (2.6b)$$

with $\ell = -\ln \Lambda/\Lambda_0$ and

$$\eta_1 = 2\pi\tilde{\kappa}, \quad (2.7a)$$

$$\eta_2 = 4\pi\tilde{\kappa}(1 + \tilde{\kappa}\tilde{\Omega}), \quad (2.7b)$$

where we introduced the rescaled dimensionless parameters

$$\tilde{\kappa} = Z_\Lambda \Lambda^{2-d}\kappa_\Lambda, \quad (2.8a)$$

$$\tilde{\Omega} = Z_\Lambda^{-2}\Lambda^{d-2}\Omega_\Lambda. \quad (2.8b)$$

These reproduce for $N = 3$ the one-loop β functions of the stiffnesses entering the NLσM given in Eq. (2.2) if one identifies $\eta_1/2 = p_3 + p_1$ and $\eta_2/4 = p_1$. One important prediction of these RG equations (which is preserved also at two-loop order [27]) is an interaction-driven enhancement of symmetry. This can be expressed by the parameter $\alpha = (p_1 - p_3)/(p_1 + p_3)$, which flows towards the fixed point $\alpha^* = 0$; i.e., all the p_i's become asymptotically equal in the IR limit $\ell \to \infty$. This signals an enhancement of the original symmetry to $O(4)/O(3)$ and this symmetry determines the critical behavior at finite ϵ in a $d = 2 + \epsilon$ expansion. We emphasize that this enhanced symmetry is, however, only expected at low temperatures and in the IR limit.

Dombre and Read [28] derived the values of the p_i's of the NLσM (2.2) appropriate for the HAFT at the original lattice scale and found $p_1 = p_2 \approx \sqrt{3}J/4T$ and $p_3 \approx 0$. This derivation was based on a local rigidity constraint where the spins were grouped into local three-spin plaquettes within which they where assumed to be rigid. We use these values to fix the derivative terms Z_{Λ_0} and Ω_{Λ_0} in our initial effective action.

While rigid rotations of the spins within a plaquette account for the three initially gapless modes, we can easily understand also the nature of the three gapped modes from looking at a single plaquette if we relax the rigidity constraint. For a local three-spin plaquette we have

$$\mathbf{S}_1 \cdot \mathbf{S}_2 + \mathbf{S}_1 \cdot \mathbf{S}_3 + \mathbf{S}_2 \cdot \mathbf{S}_3 = \boldsymbol{L}^2/2 - 3/2, \quad (2.9)$$

where $\boldsymbol{L} = \mathbf{S}_1 + \mathbf{S}_2 + \mathbf{S}_3$ is the ferromagnetic moment of the three spins, which vanishes for the planar 120° ground state. Small fluctuations around that state give rise to two massive excitations with energy $3J/4$ and a singlet with excitation $3J/2$. This is the same structure of massive modes which we obtain from Eq. (3.12), which has two modes with mass $\kappa_\Lambda \mu_\Lambda^0$ and one with mass $\kappa_\Lambda \lambda_\Lambda^0$. Dividing by the size of the unit cell $a^2\sqrt{3}/2$ (where a is the nearest-neighbor distance) we thus estimate $\mu_{\Lambda_0}^0 \kappa_{\Lambda_0} = \beta J\sqrt{3}/2$ and $\lambda_{\Lambda_0}^0 \kappa_{\Lambda_0} = \beta J\sqrt{3}$ in units such that $a = 1$ and, where Λ_0 is the UV cutoff of the model which originates from the lattice. We fix it by matching it with the smallest wave vector in the (magnetic) Brillouin zone boundary [21], $\Lambda_0 \approx 2\pi/3a$. Since we normalized the $\mathbf{\Phi}_i$ fields to be equal to one in the zero-temperature ground state, we set the initial normalization of the $\mathbf{\Phi}_i$ equal to one by choosing $\kappa_{\Lambda_0} = 1$. We finally rescale the fields to have the initial value $Z_{\Lambda_0} = 1$, the initial value of Ω_{Λ_0} is zero.

While the switch to a continuum field theory is necessarily only approximate, with this estimate of initial values of the coupling constants we nonetheless expect to get reasonable approximate values for the relevant energy scales of the model.

III. NONPERTURBATIVE RENORMALIZATION ANALYSIS OF THE LANDAU-GINZBURG MODEL

The model defined by Eq. (2.3), and extensions thereof including all local terms up to tenth order in the fields as well as two more additional derivative terms of fourth order, were investigated in Refs. [16,22]. The main objective of that analysis was to clarify the nature of the transition in $d = 3$ from the paramagnetic phase to the ordered phase, which the authors concluded was most likely of weakly first order for both $N = 2,3$. It was further shown that, already within the approximation given in Eq. (2.3), the NPRG approach

reproduces the one-loop results from a $d = 2 + \epsilon$ expansion of the NLσM, the leading term of the usual $d = 4 - \epsilon$ expansion and also the leading term of the large N expansion. They did, however, not discuss in detail the physics in $d = 2$ beyond the leading terms which recovers the one-loop NLσM result. This is the main objective of the present work.

We extend the previous truncations of the effective average action in two ways. First, studies of the BKT transition [20,23] have shown that it is important not to truncate in the power of the fields, and we therefore include local terms to arbitrary power in the invariant ρ. The reason for this is that in $d = 2$ all local terms are relevant since in $d = 2$ the engineering dimension of the fields vanishes, as measured relative to the Gaussian fixed point. Second, we extend the terms present in Eq. (2.3) to fully nonlocal ones, which effectively includes terms to arbitrary order in the spatial derivatives. This gives a more accurate approximation of the model than if one would only keep leading-order derivatives and is also not too difficult to implement. We therefore write Γ as a sum of a local and a nonlocal part,

$$\Gamma_\Lambda[\mathbf{\Phi}_1,\mathbf{\Phi}_2] = \Gamma_\Lambda^{\mathrm{loc}}[\mathbf{\Phi}_1,\mathbf{\Phi}_2] + \Gamma_\Lambda^{\mathrm{nloc}}[\mathbf{\Phi}_1,\mathbf{\Phi}_2], \tag{3.1}$$

where the local part is of the form

$$\Gamma_\Lambda^{\mathrm{loc}}[\mathbf{\Phi}_1,\mathbf{\Phi}_2] = \int_x U_\Lambda(\rho,\tau), \tag{3.2}$$

and U_Λ is a function of the two invariants ρ and τ. These two invariants are, in fact, the only local $O(N) \times O(2)$ invariants in the sense that all higher-order invariant local terms can be expressed by them [16].

A. Approximation for the local potential

Ideally, one would like to solve the full local potential exactly, which is numerically very difficult and which we therefore did not pursue. We have instead tried two different approaches, the first based on a field expansion of $U_\Lambda(\rho,\tau)$ up to eighth order in the field. However, we found that the field expansion to a given finite order does not work very well since the higher-order vertices become dominant and drive either μ_Λ or λ_Λ to negative values, which leads to a breakdown of the flow at still quite large values of Λ. This is discussed in Appendix B. In the other, more successful, approach, we approximate the local potential as $U_\Lambda(\rho,\tau) \approx V_\Lambda(\tau) + W_\Lambda(\rho)$. We then keep the full field dependence of $W_\Lambda(\rho)$, but approximate $V_\Lambda(\tau)$ by its leading term in a field expansion,

$$U_\Lambda(\rho,\tau) \approx \mu_\Lambda^0 \tau/4 + W_\Lambda(\rho). \tag{3.3}$$

This choice is based on the assumption that the ρ dependence of the local potential is more important than the τ dependence since it controls the symmetry-breaking expectation value κ_Λ. Within such an ansatz, one avoids the problems coming from the large higher-order terms which appear in a finite-order field expansion. Note that such a scheme could also be carried out to a higher order in τ, which, at least for smaller powers of τ, would be significantly less numerically demanding than keeping the full local potential. Here, however, we limit the analysis to the approximation (3.3).

B. Approximation of the nonlocal terms

The nonlocal part contains terms up to quartic order in the fields and, as a direct generalization of Eq. (2.3), is approximated as

$$\begin{aligned}\Gamma_\Lambda^{\mathrm{nloc}}[\mathbf{\Phi}_1,\mathbf{\Phi}_2] = {}& \frac{1}{2}\int_k z_\Lambda(k)[\mathbf{\Phi}_{1,k}\cdot\mathbf{\Phi}_{1,-k} + \mathbf{\Phi}_{2,k}\cdot\mathbf{\Phi}_{2,-k}] \\ & + \frac{1}{4}\int_{x,x'} \lambda_\Lambda(x-x')[\rho_x/2-\kappa_\Lambda][\rho_{x'}/2-\kappa_\Lambda] \\ & + \frac{1}{4}\int_{x,x'} \frac{\mu_\Lambda(x-x')}{2}\mathrm{Tr}\mathcal{A}_x\mathcal{A}_{x'} \\ & - \frac{1}{8}\int_{x,x'} \omega_\Lambda(x-x') \\ & \times[\mathbf{\Phi}_1(x)\cdot\mathbf{\Phi}_2(x') - \mathbf{\Phi}_2(x)\cdot\mathbf{\Phi}_1(x')]^2, \end{aligned} \tag{3.4}$$

where $\int_k = (2\pi)^{-d}\int d^dk$, $\rho_x = \mathbf{\Phi}_{1,x}^2 + \mathbf{\Phi}_{2,x}^2$ is the x-dependent "density" which measures the local fluctuating moment of the 120° magnetization, and $\mathcal{A}_x = {}^t\Phi_x\Phi_x - \mathbb{1}\rho_x/2$ are x-dependent matrices. The μ part of the action can also be written as

$$\begin{aligned}\tfrac{1}{2}\mathrm{Tr}\mathcal{A}_x\mathcal{A}_{x'} = {}& \left(\mathbf{\Phi}_{1,x}^2 - \mathbf{\Phi}_{2,x}^2\right)\left(\mathbf{\Phi}_{1,x'}^2 - \mathbf{\Phi}_{2,x'}^2\right)/4 \\ & + \mathbf{\Phi}_{1,x}\cdot\mathbf{\Phi}_{2,x}\,\mathbf{\Phi}_{1,x'}\cdot\mathbf{\Phi}_{2,x'}. \end{aligned} \tag{3.5}$$

The coupling functions z_Λ, μ_Λ, λ_Λ, and Ω_Λ are all defined to be completely nonlocal; i.e., after a Fourier transform they have a vanishing contribution at momentum $k = 0$. The local contributions are included in U_Λ and will be denoted by μ_Λ^0 and λ_Λ^0. For later convenience we also introduce the functions

$$\bar{\mu}_\Lambda(k) = \mu_\Lambda(k) + \mu_\Lambda^0, \tag{3.6a}$$

$$\bar{\lambda}_\Lambda(k) = \lambda_\Lambda(k) + \lambda_\Lambda^0. \tag{3.6b}$$

The derivative terms present in the action (2.3) correspond to the approximation

$$z_\Lambda(k) = Z_\Lambda k^2 + \mathcal{O}(k^4), \tag{3.7a}$$

$$\omega_\Lambda(k) = \Omega_\Lambda k^2 + \mathcal{O}(k^4), \tag{3.7b}$$

and $\mu_\Lambda(k) = \lambda_\Lambda(k) = 0$. To keep also the leading-order k^2 terms of $\mu_\Lambda(k)$ and $\lambda_\Lambda(k)$ is equivalent to introducing the derivative terms

$$\begin{aligned}&(\mathbf{\Phi}_1\cdot\partial_x\mathbf{\Phi}_1 + \mathbf{\Phi}_2\cdot\partial_x\mathbf{\Phi}_2)^2, \\ &(\mathbf{\Phi}_1\cdot\partial_x\mathbf{\Phi}_1 - \mathbf{\Phi}_2\cdot\partial_x\mathbf{\Phi}_2)^2 + (\mathbf{\Phi}_1\cdot\partial_x\mathbf{\Phi}_2 + \mathbf{\Phi}_2\cdot\partial_x\mathbf{\Phi}_1)^2,\end{aligned}$$

in the action (2.3).

C. Derivation of the flow equations

The NPRG is based on an exact flow equation for the effective average action $\Gamma_\Lambda[\Phi]$ [29],

$$\partial_\Lambda\Gamma_\Lambda[\Phi] = \frac{1}{2}\mathrm{Tr}\left[\partial_\Lambda R_\Lambda\left(\frac{\partial^2\Gamma_\Lambda}{\partial\Phi\partial\Phi} + R_\Lambda\right)^{-1}\right], \tag{3.8}$$

where the trace is over momenta and internal indices. For notational brevity we omitted internal indices and momenta in the field derivatives as well as in R_Λ in Eq. (3.8). Note that the

second-order field derivative of Γ_Λ on the right-hand side in Eq. (3.8) is also a functional of the field Φ. If both sides of this equation are expanded in the fields, one obtains flow equations for the irreducible vertices. The derivation of Eq. (3.8) is based on an approach where the cutoff is introduced into the model via a regulator R_Λ, which is added to the bare two-point function. At the initial UV scale Λ_0, the action is assumed to be the bare one, whereas the full irreducible vertices are obtained from Eq. (3.8) when the flow of Γ_Λ is integrated from $\Lambda = \Lambda_0$ down to $\Lambda = 0$. While Eq. (3.8) is exact, it is almost always impossible to solve it exactly and approximation techniques are required. The most common ones are either based on an expansion of Γ_Λ to a finite order in the fields or an expansion in the derivatives; for reviews, see, e.g., [16,23,24]. Here we use a combination of both, where we take into account both terms which are not restricted to a finite order in the fields but also nonlocal terms to arbitrarily order in the derivatives [30]. The regulator R_Λ removes IR divergent terms arising from modes with $k < \Lambda$ and for numerical stability we use an analytic regulator. A standard choice [23] is

$$R_\Lambda(q) = Z_\Lambda \frac{q^2}{\exp(q^2/\Lambda^2) - 1}. \tag{3.9}$$

The flow equations are most easily derived in a basis where the two-point functions are diagonal. Following Ref. [16] we therefore first introduce the two N-component fields $\boldsymbol{\Phi}_a(x) = \boldsymbol{\varphi}_a(x) + \boldsymbol{\chi}_a$, where $\boldsymbol{\chi}_a$ are the finite expectation values which we assume to have the form

$$^t\boldsymbol{\chi}_1 = \left(\kappa_\Lambda^{1/2}, 0, \ldots, 0\right), \tag{3.10a}$$

$$^t\boldsymbol{\chi}_2 = \left(0, \kappa_\Lambda^{1/2}, 0 \ldots, 0\right). \tag{3.10b}$$

Diagonalization of the two-point functions is achieved by a switch to the basis $\tilde{\varphi}_a^\alpha$ (with $a = 1,2$ and $\alpha = 1, \ldots, N$),

$$\tilde{\varphi}_1^1 = \frac{1}{\sqrt{2}}\left(\varphi_1^1 + \varphi_2^2\right), \tag{3.11a}$$

$$\tilde{\varphi}_2^1 = \frac{1}{\sqrt{2}}\left(\varphi_1^1 - \varphi_2^2\right), \tag{3.11b}$$

$$\tilde{\varphi}_1^2 = \frac{1}{\sqrt{2}}\left(\varphi_1^2 + \varphi_2^1\right), \tag{3.11c}$$

$$\tilde{\varphi}_2^2 = \frac{1}{\sqrt{2}}\left(\varphi_1^2 - \varphi_2^1\right), \tag{3.11d}$$

and $\tilde{\varphi}_a^\alpha = \varphi_a^\alpha$ for $\alpha > 2$. In the rotated basis only one component has a finite expectation value, $\tilde{\chi}_\alpha^a = \sqrt{2\kappa_\Lambda}\delta_{a1}\delta_{\alpha 1}$. The two-point vertices are now diagonal in the a,α space and have the form

$$\begin{aligned}\Gamma_{ab}^{\alpha\beta}(k) &= \frac{\partial^{(2)}}{\partial\tilde{\varphi}_a^\alpha(k)\tilde{\varphi}_b^\beta(-k)}\Gamma_\Lambda|_{\varphi=0} \\ &= \delta_{ab}\delta_{\alpha\beta}\{z_\Lambda(k) + \kappa_\Lambda[\delta_{a,1}\delta_{\alpha,1}\bar{\lambda}_\Lambda(k) + \eta_{a\alpha}\bar{\mu}_\Lambda(k) \\ &\quad + \delta_{a,2}\delta_{\alpha,2}\omega_\Lambda(k)]\},\end{aligned} \tag{3.12}$$

where we introduced $\eta_{a\alpha}$, which has as nonzero entries only $\eta_{12} = \eta_{21} = 1$. The functions $\bar{\mu}_\Lambda(k)$ and $\bar{\lambda}_\Lambda(k)$ are defined in Eqs. (3.6).

The flow of the local potential is obtained by evaluating Eq. (3.8) for constant fields [23]. The initial form of the local potential at $\Lambda = \Lambda_0$ coincides with the interaction term of the bare action and is given by $U_{\Lambda_0} = \lambda^0_{\Lambda_0}(\rho/2 - \kappa_{\Lambda_0})^2/4 + \mu^0_{\Lambda_0}\tau/4$. The flow of the local terms present in the two-parameter function U_Λ is greatly simplified if we employ the approximation Eq. (3.3). The flow of $W_\Lambda(\rho)$ is then found to be

$$\partial_\Lambda W_\Lambda(\rho) = \frac{1}{2}\int_k \partial_\Lambda R_\Lambda(k) \sum_{a=1,2,\alpha=1,\ldots,N} G_\Lambda^{a\alpha}(k,\rho), \tag{3.13}$$

with

$$G_\Lambda^{11}(k,\rho) = [A_\Lambda(q,\rho) + \rho W_\Lambda''(\rho) + \rho\lambda_\Lambda(q)/2]^{-1}, \tag{3.14a}$$

$$G_\Lambda^{12}(k,\rho) = [A_\Lambda(q,\rho) + \rho\bar{\mu}_\Lambda(q)/2]^{-1}, \tag{3.14b}$$

$$G_\Lambda^{22}(k,\rho) = [A_\Lambda(q,\rho) + \rho\Omega_\Lambda(q)/2]^{-1}. \tag{3.14c}$$

The remaining functions are $G_\Lambda^{21}(k,\rho) = G_\Lambda^{12}(k,\rho)$ and there are $2(N-2)$ modes of the form $G_\Lambda^{a\alpha} = A_\Lambda(q,\rho)^{-1}$ for $\alpha > 2$, with

$$A_\Lambda(q,\rho) = R_\Lambda(q) + z_\Lambda(q) + W_\Lambda'(\rho). \tag{3.15}$$

The flow of κ_Λ is obtained from the requirement that $(d/d\Lambda)W'(\rho = 2\kappa_\Lambda) = 0$, i.e., that κ_Λ is for all Λ the position of the minimum of W_Λ [23].

To solve the flow equations numerically, we need to have an accurate resolution of the local potential around the flowing minimum κ_Λ. Since for $d = 2$ this minimum vanishes for $N \geqslant 3$ at some finite Λ^*, reflecting the finite correlation length, we need to rescale the local potential. This is achieved by writing

$$W_\Lambda(\rho) = \kappa_\Lambda^2 w_\Lambda(y = \rho/\kappa_\Lambda) \tag{3.16}$$

so that the rescaled potential $w_\Lambda(y)$ always has its minimum at $y = 2$. Choosing a linear grid for y proved then sufficient to obtain converged and stable flows. At low temperatures, $w_\Lambda(y)$ rapidly approaches a convex form and becomes essentially flat for $y < 2$.

To derive the flow equations of the nonlocal terms in Γ_Λ, i.e., of the functions $\mu_\Lambda(k)$, $\lambda_\Lambda(k)$, and $\Omega_\Lambda(k)$, we invoke a field expansion [23,24]. We need the vertices up to fourth order in an expansion in $\tilde{\varphi}_a^\alpha$; they can be found in Appendix A. From the explicit form of all vertex functions up to the four-point vertex, we can determine the flows of the nonlocal coupling functions directly from the standard flows of the two-particle vertices using Eq. (3.12), this is discussed in detail in Ref. [30] and, in connection with membranes [31], by the first two works in Ref. [31]. The flow of the self-energy $\Gamma_{11}^{22}(k=0)$ also yields the flow of the local coupling constant μ_Λ^0. We emphasize that the obtained flow equations are uniquely determined by the effective average action specified through Eqs. (3.1)–(3.4). The flow equations are rather lengthy and not very illuminating, and we therefore do not present them here. For an alternative approach to include the momentum dependence of vertices, which is not based on a truncation of the effective average action but on an approximation at the level of a field expansion in presence of a background field; see Refs. [32].

IV. RESULTS AND DISCUSSION

We have integrated the NPRG flow equations corresponding to Eqs. (3.1)–(3.4) for different temperatures, ranging from $T = 0.6J$ down to $T = 0.24J$. The lower the temperature, the smaller the logarithmic step size $\delta\ell$ (with $\ell = -\ln \Lambda/\Lambda_0$) had to be chosen in the partial differential equation solver routine. If $\delta\ell$ is chosen too large in comparison with the discretization δy in the representation of the local potential $w_\Lambda(y)$, small oscillations in the derivatives of $w_\Lambda(y)$ appear, which quickly grow and lead to numerical instabilities. Thus, we had to choose rather small step sizes at low temperatures, down to $\delta\ell \simeq 4 \times 10^{-5}$ for $T = 0.24J$, and we could not reach arbitrarily low temperatures since at $T \leqslant 0.24J$ it takes already more than 1 week to calculate the flow for a given temperature (using a single core of the CPU). We also note that an adaptive step solver turned out to be problematic since it generally cannot cope well with the instabilities which arise at larger step sizes.

We are interested in the spin-correlation length ξ which characterizes the decay of the spin correlation function $\langle \boldsymbol{S}_{x_i} \cdot \boldsymbol{S}_{x_j} \rangle$, where x_i and x_j belong to the same sublattice of the 120° order. The relations (2.5) imply that $\langle \boldsymbol{\Phi}_x \cdot \boldsymbol{\Phi}_y \rangle$ decays with the same correlation length as $\langle \boldsymbol{S}_{x_i} \cdot \boldsymbol{S}_{x_j} \rangle$. We can thus extract the spin correlation length directly from our NPRG analysis as the scale Λ^* where the order parameter κ_{Λ^*} vanishes. In Fig. 1 we show results for ξ as a function of temperature. At low temperatures the correlation length grows exponentially and follows a $\xi \approx \exp BJ/T$ behavior. We compare this with the correlation length of the NLσM applied to the HAFT, which, at two-loop order, has the form [27]

$$\xi_{\mathrm{HAFT}}/a \approx C_\xi \sqrt{T/J} \exp(6.9943 J/T), \tag{4.1}$$

with an undetermined constant C_ξ. The exponent $B = 6.9943$ is the same also in the one-loop approximation. Our NPRG analysis yields the slightly smaller value $B \approx 6$. As we discuss in more detail below, the NPRG flow deviates from the NLσM flow already at moderate temperatures and also at small spatial scales, although they do coincide at small temperatures and large scales. Since the NLσM prediction for $\xi(T)$ is based on the integration of the flow equation starting from the lattice scale, a small deviation of the correlation length exponent B is not unexpected.

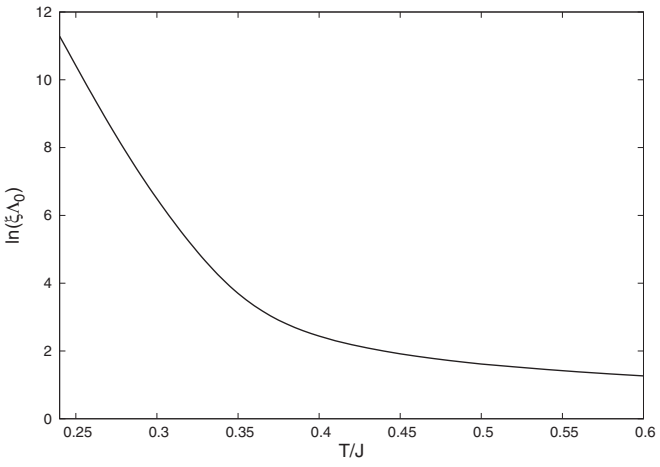

FIG. 1. The correlation length as a function of temperature has an exponential dependence on the temperature but a much weaker temperature dependence at larger temperature, with a crossover temperature of $T \approx 0.35J$ separating the two regimes.

What can be clearly observed is a pronounced crossover at around $T_{\mathrm{cross}} \approx 0.35J$, from the low-temperature exponential temperature dependence to a much more modest decay of ξ at larger temperatures. This crossover happens in a relatively narrow temperature range, yet $\xi(T)$ is smooth and continuous, with no sign of an underlying thermodynamic singularity. This crossover is similar to the sharp increase of the correlation length seen in MC simulations for temperatures $T \lesssim 0.3J$ [5,18]. The finite size limitations in MC combined with the exponential growth of the correlation length, however, make it difficult to obtain converged results for $\xi(T)$ from MC and it was not clear if $\xi(T)$ or its temperature derivative would be smooth in the thermodynamic limit. A recent theory [6] has proposed that the spin correlation length is a convolution of two correlation lengths, $\xi = \xi_v \xi_{sw}/(\xi_v + \xi_{sw})$. The vortex correlation length ξ_v is assumed to diverge at a finite temperature T_c while the spin-wave correlation length ξ_{sw} remains finite for all $T > 0$. The resulting form of the magnetic correlation length would have a nonmonotonic function $d \ln(\xi \Lambda_0)/dT$ with a maximum near T_c. Our NPRG analysis does not show such a behavior. We emphasize that this crossover cannot be obtained within a NLσM approach and neither in a finite order field expansion, as discussed in Appendix B.

The flow of the free energy can also readily be obtained from our analysis, it corresponds to the flow of Γ_Λ evaluated at $\rho = 2\kappa_\Lambda$ and $\tau = 0$. Thus, the flow of the free energy follows from Eq. (3.13) with $\rho = 2\kappa$. As a result of keeping the nonlocal coupling functions $\mu_\Lambda(k)$, $\lambda_\Lambda(k)$, and $\Omega_\Lambda(k)$ in our analysis, the thus evaluated free energy is sensitive to a broad range of energy scales beyond the IR limit. Since the NPRG breaks down at some finite scale Λ^* where $\kappa_{\Lambda^*} = 0$, we cannot follow the free energy flow down to $\Lambda = 0$. To extract the contributions to the free energy coming from $0 < \Lambda < \Lambda^*$, we took advantage of the fact that all propagators are gapped in this regime because of the finite correlation length ξ and thus no IR divergences are present. We therefore approximated the propagators in this regime simply by introducing a finite correlation length $\xi^{-1} = 2\pi\Lambda^*$ into the self-energies and by replacing all flow parameters by their values at $\Lambda = \Lambda^*$. We note that the region $\Lambda < \Lambda^*$ contributes only a very small fraction to the total free energy at low temperatures, which has no noticeable effect on the shape of the specific heat in the temperature range considered here. From the thus-obtained free energy we calculate the specific heat $C = -T(\partial^2 f/\partial T^2)$, which required some local smoothing of the $f(T)$ data to avoid noise in $C(T)$. Our result for $C(T)$ is plotted in Fig. 2 and shows a well-defined but relatively broad peak, again rather similar to what is obtained from MC simulations [6]. While the specific heat typically shows a singularity near a second-order phase transition with a divergent correlation length, the broad peak observed here is a consequence of the rapid crossover of the spin correlation length in that temperature regime rather than a true divergence.

The behavior of both the correlation length and the specific heat thus suggest that there is no true phase transition at T_{cross}

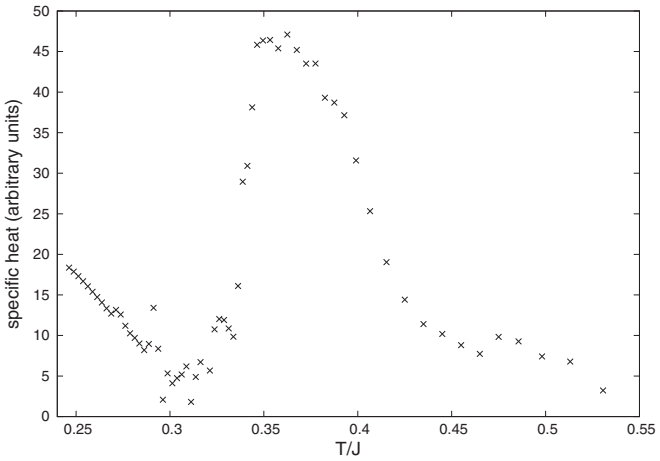

FIG. 2. The specific heat as a function of temperature. It shows a well-defined broad peak in the same temperature range where the correlation length $\xi(T)$ has the crossover.

but rather a crossover from a purely spin-wave-dominated regime (the NLσM regime) to a high-temperature regime where defects and massive excitations play an important role. This picture is also supported by comparing our NPRG flow to the one obtained from the NLσM. In Fig. 3 we show the flow of the two parameters η_1 and η_2 from the NPRG and for the NLσM, at different temperatures. Since we have data from the full NPRG flow only down to $T = 0.24J$, we also show data obtained from the derivative expansion of Γ_Λ, using only the parameters which enter in Eq. (2.3). In the limit of large masses λ_Λ^0 and μ_Λ^0 the NPRG flow equations in the derivative expansion approximation reduce to the one-loop NLσM flow [16]. This is clearly seen at $T = 0.12J$. However, the large mass limit of the flow equations is reached only very slowly and at moderately small temperatures finite-mass corrections are visible. Already at $T = 0.18J$ one sees deviations from both the one-loop and the two-loop NLσM flow, which become quite substantial at $T = 0.24J$. At this temperature we have calculated the NPRG flow both in the full approximation, corresponding to Eqs. (3.3) and (3.4), as well as in the derivative approximation (2.3). Both NPRG flows show similar deviations from the NLσM results. The deviations grow at even larger temperatures when compared to the full NPRG flow. At $T = 0.30J$, η_1 and η_2 vanish at a Λ scale where the NLσM results still predict sizeable finite stiffnesses.

The crossover at T_{cross} has often been argued to be caused by unbound Z_2 defects which start to proliferate at T_{cross} [4,6]. MC simulations have found evidence of a vortex unbinding at this temperature. Southern and Xu [4] have extracted a vorticity modulus from their MC data which was shown to vanish near T_{cross}, which was interpreted as an unbinding of vortices. While the spin stiffness is always zero for any $T > 0$, in finite-sized systems the spin stiffness vanishes only at sufficiently large T. For system sizes comparable to those of Ref. [4] the spin stiffness vanishes at roughly the same T as the vorticity modulus [5]. The vortex unbinding at low temperatures is prevented by a logarithmic interaction among the vortices which is, however, only present for length scales smaller than

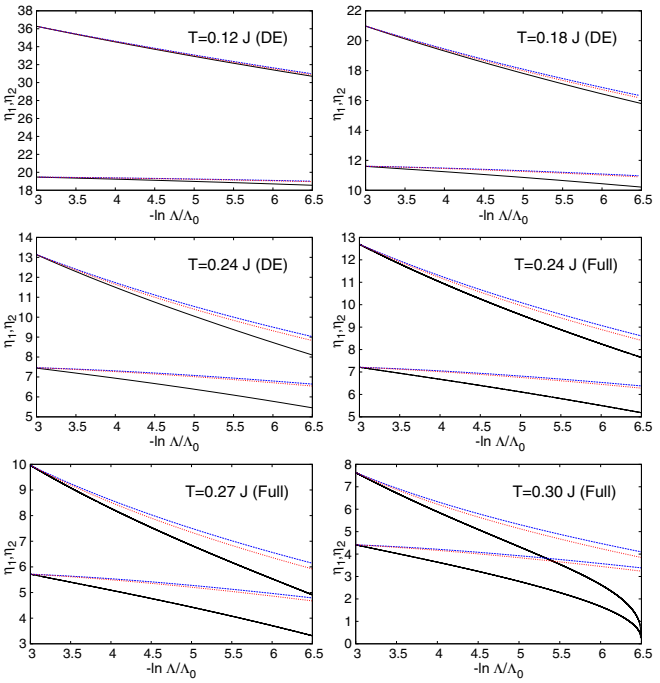

FIG. 3. (Color online) Flow of the parameters η_1, η_2 (with $\eta_2 > \eta_1$), from NPRG calculations (solid black lines) and from perturbative one-loop (dotted blue lines) and perturbative two-loop (dashed red lines) RG calculations for the NLσM. For the NLσM $\eta_{1,2}$ are the spin stiffnesses, whereas for the NPRG we extracted $\eta_{1,2}$ via Eqs. (2.7a) and (2.7b). For low temperatures $T \leqslant 0.24J$ the NPRG flows are those of the derivative expansion (DE) [see (2.3), whereas for $T \geqslant 0.24J$ we show the flow calculated in the full approximation Eqs. (3.1)–(3.4). The one- and two-loop NLσM results are always very similar and strongly overlap in the plots for $T \leqslant 24$. For $T = 0.12$ all approximations strongly overlap.

the correlation length [33]. To gain further insight into the physics behind the crossover, we plot the flowing anomalous dimension η. For a true second-order phase transition $\xi \to \infty$ and η would become a critical exponent. It characterizes the spin-spin correlation function at criticality, which behaves for $k \to 0$ as $1/k^{2-\eta}$. Here for any finite T the spin correlation length is finite and η does not reach a constant for $k \to 0$. Yet, for low temperatures, η changes only very modestly for momenta $k < 1/\xi$ and both ξ and $2\pi/k$ much larger than the microscopic lattice spacing. The scale-dependent anomalous dimension η is defined through

$$\eta = \Lambda \partial_\Lambda \ln Z_\Lambda. \tag{4.2}$$

We plot it as a function of the rescaled order parameter $\tilde{\kappa}$, defined in Eq. (2.8a), for different temperatures in Fig. 4. For the XY model, these plots show a characteristic flow which, for temperatures below the critical one, quickly reaches a line of $\eta(\tilde{\kappa})$, where the flow of $\tilde{\kappa}$ essentially stops [20]. This line signifies thus a line of fixed points where the anomalous dimension reaches a finite value for $\Lambda \to 0$. The line of fixed points terminates around a value $\eta = 0.287$, beyond which the flow is away from the line of fixed points. What we find in the present model is in some ways similar to the XY flow, however with important differences. At low temperatures we

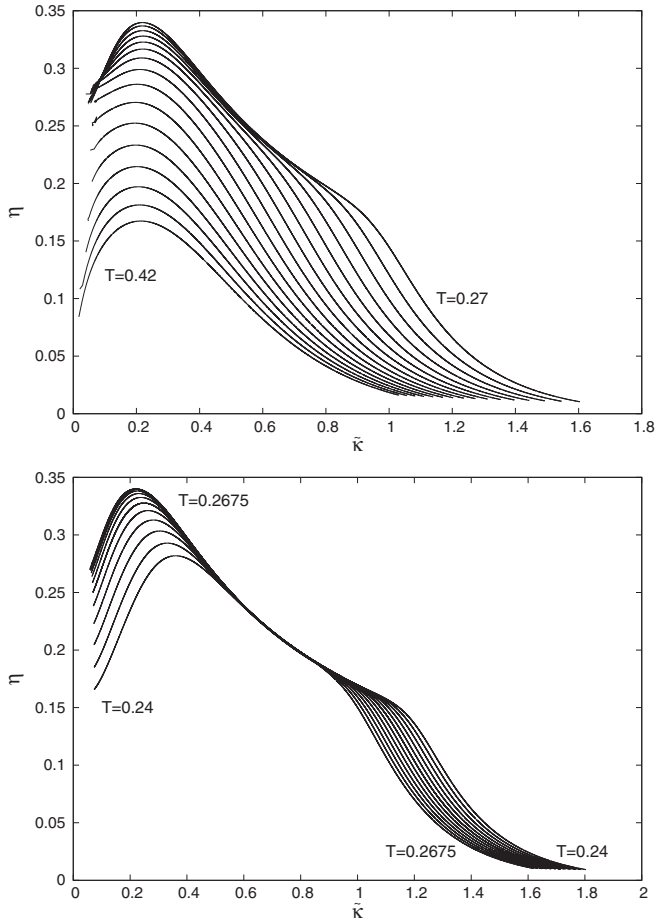

FIG. 4. Anomalous exponent η vs the rescaled order parameter $\tilde{\kappa}$. The upper curve shows results for large temperatures; the lower curve shows results at smaller temperatures.

do find a common curve $\eta(\tilde{\kappa})$ to which all flows are attracted. However, while the flow along this line is slower than the initial approach to that line, the flow never stops but remains sizable, in accordance with the asymptotic freedom of the model. Thus, one never actually reaches a fixed point and no transition or critical behavior can be associated with the common curve.

The maximal value of $\eta_{\max} \approx 0.34$, is close to the value $\eta_{\max} \approx 0.33$ found in the XY model (the line of fixed point ends in the XY model at a smaller value ≈ 0.287, rather close to the exact value $1/4$). This may be seen as an indication that indeed some enhanced stability against defect unbinding exist along the line $\eta(\tilde{\kappa})$. In this interpretation, for temperatures lower than roughly $T \approx 0.27J$, a large part of the flow is along the common curve $\eta(\tilde{\kappa})$ and only at sufficiently small Λ it deviates, owing to the vanishing of the order parameter and the appearance of a finite correlation length. While defects would certainly be present at scales larger than the correlation length, the fact that the maximal value of η systematically decreases with lowering the temperature below $T = 0.27J$ indicates a stability against vortex unbinding. Thus, the correlation length in this regime is limited by the asymptotic freedom of the model rather than an unbinding of vortices. The stability to vortices (for scales smaller than the correlation length) is then similar to the XY model where along the critical line $T < T_c$ the anomalous dimension reaches a fixed point whose value is proportional to the temperature. We also find that over a large momentum range the spin correlation decay is algebraic with anomalous exponents and only at large distances does the finite correlation length induce an exponential decay.

At larger temperatures (see the upper plot in Fig. 4), the flow starts to deviate slowly from the common curve $\eta(\tilde{\kappa})$ of the low-temperature regime. At around $T \approx 0.30J$ it never reaches it and moves further away from it the higher the temperature. This indicates that at these temperatures the regime where gapless excitations dominate the flow is never reached and massive and/or topological excitations become ubiquitous. For $T = 0.35$ the maximum is approximately $\eta = 0.28$, similar to the NPRG estimate of the critical temperature of the XY model. All this is consistent with a correlation length which is, at high temperatures, primarily determined by a vortex unbinding. That the correlation lengths actually decrease more slowly at higher temperatures where vortices are abundant, as is also observed in MC simulation [5,18], can be understood on the grounds that the flow ceases to be controlled by the low-temperature NLσM model and its strong, asymptotic freedom-dominated temperature dependence of the correlation length.

Thus, we see in the flow of η support for the scenario of vortex unbinding somewhere in the temperature interval $0.3J$–$0.35J$, where also the crossover in the correlation length dependence on temperature is observed. In the NPRG we have, however, no direct access to vortex degrees of freedom, so that we can only say that our results are consistent with a vortex unbinding scenario.

V. SUMMARY

We have analyzed two-dimensional frustrated Heisenberg magnets within a NPRG framework, using initial values for the flow as appropriate for the antiferromagnetic Heisenberg model on the triangular lattice. We follow the general NPRG approach for frustrated magnets as developed in Refs. [16,22], which makes it possible to recover the NLσM flow equations at sufficiently low temperatures. We extend this analysis in two ways: Instead of expanding the action to a given order in a field expansion, we keep the full local dependence of the effective action on the invariant ρ, which is the local fluctuating magnitude of the ordered moments of the magnet. Further, we replace the coupling parameters of the standard Landau-Ginzburg action with nonlocal coupling functions.

The primary goal of our analysis is to clarify the nature of the finite temperature crossover in the correlation length dependence of the MC simulations of the HAFT at around a temperature $T \approx 0.3J$ and to investigate a possible role of topological defects. Our analysis reproduces the key feature of the MC simulations. As expected, at low temperatures we recover the flow of the NLσM which was shown to be in accordance with MC simulations in Refs. [5,18]. The NPRG flow deviates further and further from the NLσM predictions upon increasing the temperature and we find a crossover of the temperature dependence of the correlation length at around $T_{\text{cross}} \approx 0.35J$. Although this temperature is slightly larger than the one observed in MC, which is not surprising in view of the approximations inherent in the mapping of the lattice model into a continuum theory, our NPRG approach

does capture the crossover qualitatively. The specific heat, which shows a broad peak around the crossover, is also in qualitative agreement with MC simulations [6]. As discussed in Sec. IV closer inspection of the flow of the anomalous dimension shows that for temperatures slightly lower than T_{cross} the flows collapse over a wide range of scales on a common curve $\eta(\tilde{\kappa})$, where $\tilde{\kappa}$ is the rescaled local-order parameter. In this regime the (large) correlation length arises from the asymptotic freedom of the model and thus from the geometry of the order parameter space. In contrast, at around temperatures $0.3J$–$0.35J$, the flow starts to deviate from the common curve $\eta(\tilde{\kappa})$. The maximal anomalous dimension is reached around this temperature and is similar to that of the XY model at the vortex unbinding transition. While a topological origin of this behavior is plausible, we find no indication of a finite temperature fixed point and all our results are instead consistent with a crossover. Physically, this is not completely unexpected since a true phase transition would usually require a logarithmic interaction among the vortices, as it occurs within the BKT scenario. In view of the finite correlation length the logarithmic interaction is cut off at large distances, which would result in a crossover rather than a phase transition, and there would be no diverging length scale associated with the crossover. How can this be reconciled with the presence of two phase transitions which are clearly observed in MC simulations at small but finite fields [7,8]? A likely scenario is that for vanishing fields the two critical points meet and merge into a crossover point instead. This is consistent with the vanishing of the order parameters of both low-temperature phases in the zero-field limit [7]. Further analysis of the low-field regime with the NPRG would certainly be desirable.

ACKNOWLEDGMENTS

We thank Federico Benitez, Nic Shannon, Dominique Mouhanna, and Lorenz Bartosch for discussions and suggestions. N.H. acknowledges support from the DFG research group FOR 723.

APPENDIX A: FORM OF HIGHER-ORDER VERTICES

Here we give the expressions for the symmetrized vertices which are required to derive the flow equations of the nonlocal coupling functions. Besides the two-point vertex, given in Eq. (3.12), these are the three- and four-point vertices. The three-point vertex, in the basis defined in Eqs. (3.11), is

$$\begin{aligned}\Gamma^{\alpha_1\alpha_2\alpha_3}_{a_1a_2a_3}(\boldsymbol{k}_1,\boldsymbol{k}_2,\boldsymbol{k}_3) = \sqrt{\kappa/2}\big\{&\big[\delta_{a_11}\delta_{\alpha_12}\big(\delta^{>}_{\alpha_2\alpha_3}\eta_{a_2a_3}+\eta_{\alpha_2\alpha_3}\delta_{a_2a_3}\xi_{a_2}\big)+\delta_{a_12}\delta_{\alpha_11}\big(\delta^{>}_{\alpha_2\alpha_3}\delta_{a_2a_3}\xi_{a_2}+\delta^{<}_{\alpha_2\alpha_3}\eta_{a_2a_3}\big)\big]\mu(k_1)\\ &+\delta_{a_11}\delta_{\alpha_11}\delta_{a_2a_3}\delta_{\alpha_2\alpha_3}\big[\lambda(k_1)+32\kappa U'''_\Lambda(\rho=2\kappa)\delta_{a_21}\delta_{\alpha_21}\big]\\ &+\delta_{a_12}\delta_{\alpha_12}\epsilon_{a_2a_3}\big[\delta_{\alpha_2\alpha_3}-\Theta(\alpha_2\leqslant 2)\Theta(\alpha_3\leqslant 2)\big][\Omega(k_2)-\Omega(k_3)]+(1\leftrightarrow 2)+(1\leftrightarrow 3)\big\},\end{aligned}\tag{A1}$$

where $\delta^{<}_{\alpha\beta}=\delta_{\alpha\beta}\Theta(\alpha\leqslant 2)$, and $\delta^{>}_{\alpha_\beta}=\delta_{\alpha\beta}\Theta(\alpha>2)$. We further defined the vector $\xi_a=(1,-1)^t$ and $\epsilon_{ab}=-\epsilon_{ba}$ is the antisymmetric tensor with $\epsilon_{12}=1$. The tensor $\eta_{a\alpha}$ has nonzero entries only for $\eta_{12}=\eta_{21}=1$. The notation $(1\leftrightarrow 2)$ is short for $(k_1,a_1,\alpha_1\leftrightarrow k_2,a_2,\alpha_2)$. The four-point vertex in the basis defined in Eqs. (3.11) is

$$\begin{aligned}\Gamma^{\alpha_1,\ldots,\alpha_4}_{a_1,\ldots,a_4}(\boldsymbol{k}_1,\ldots,\boldsymbol{k}_4) = \tfrac{1}{2}\big\{&\big[\big(\eta_{a_1a_2}\delta^{>}_{\alpha_1\alpha_2}+\delta_{a_1a_2}\xi_{a_1}\eta_{\alpha_1\alpha_2}\big)\big(\eta_{a_3a_4}\delta^{>}_{\alpha_3\alpha_4}+\delta_{a_3a_4}\xi_{a_3}\eta_{\alpha_3\alpha_4}\big)\\ &+\big(\delta_{a_1a_2}\delta^{>}_{\alpha_1\alpha_2}\xi_{a_1}+\eta_{a_1a_2}\delta^{<}_{\alpha_1\alpha_2}\big)\big(\delta_{a_3a_4}\delta^{>}_{\alpha_3\alpha_4}\xi_{a_3}+\eta_{a_3a_4}\delta^{<}_{\alpha_3\alpha_4}\big)\big]\mu(k_{12})\\ &+\delta_{a_1a_2}\delta_{a_3a_4}\delta_{\alpha_1\alpha_2}\delta_{\alpha_3\alpha_4}\big[\lambda(k_{12})+32\kappa U'''_\Lambda(\rho=2\kappa)\big(\delta_{a_11}\delta_{\alpha_11}+\delta_{a_31}\delta_{\alpha_31}\big)\\ &+128\kappa^2U''''_\Lambda(\rho=2\kappa)\delta_{a_11}\delta_{a_32}\delta_{\alpha_11}\delta_{\alpha_31}\big]+\big[\delta_{\alpha_1\alpha_2}-\Theta(\alpha_1\leqslant 2)\Theta(\alpha_2\leqslant 2)\big]\\ &\times\big[\delta_{\alpha_3\alpha_4}-\Theta(\alpha_3\leqslant 2)\Theta(\alpha_4\leqslant 2)\big]\epsilon_{a_1a_2}\epsilon_{a_3a_4}[\Omega(k_{14})-\Omega(k_{13})]+(1\leftrightarrow 3)+(1\leftrightarrow 4)\big\}.\end{aligned}\tag{A2}$$

APPENDIX B: FIELD EXPANSION OF LOCAL POTENTIAL

Here we discuss the flow equations if we approximate the local potential $U_\Lambda(\rho,\tau)$ up to eighth order in the fields. To that order, we have, up to a field-independent constant,

$$\begin{aligned}U_\Lambda(\tau,\rho/2-\kappa) = \int_x\Big[&\frac{\lambda^0_\Lambda}{4}(\rho/2-\kappa)^2+\frac{\mu^0_\Lambda}{4}\tau+\frac{c^{(3)}_\rho}{12}(\rho/2-\kappa)^3\\ &+\frac{c_{\rho\tau}}{8}(\rho/2-\kappa)\tau+\frac{c^{(4)}_\rho}{24}(\rho/2-\kappa)^4\\ &+\frac{c^{(2)}_\tau}{32}\tau^2+\frac{c^{(2)}_{\rho\tau}}{16}(\rho/2-\kappa)^2\tau\Big].\end{aligned}\tag{B1}$$

Higher-order terms can be readily included, but the resulting flow equations become rather long if the full k dependence of the coupling functions $\mu_\Lambda(k)$, $\lambda_\Lambda(k)$, and $\Omega_\Lambda(k)$ is kept. To compare the different approximations, we introduce the rescaled and (in $d=2$) dimensionless local coupling parameters

$$\tilde{\mu}=\mu^{(0)}_\Lambda\Lambda^{-2}Z_\Lambda^{-2},\tag{B2a}$$

$$\tilde{\lambda}=\lambda^{(0)}_\Lambda\Lambda^{-2}Z_\Lambda^{-2}.\tag{B2b}$$

In Fig. 5 we show the flow of $\tilde{\lambda}$ from the field expansion to both order Φ^6 [setting $c^{(4)}_\rho$, $c^{(2)}_\tau$, and $c^{(2)}_{\rho\tau}$ equal to zero in Eq. (B1) and order Φ^8. In both cases $\tilde{\lambda}$ is driven rapidly to

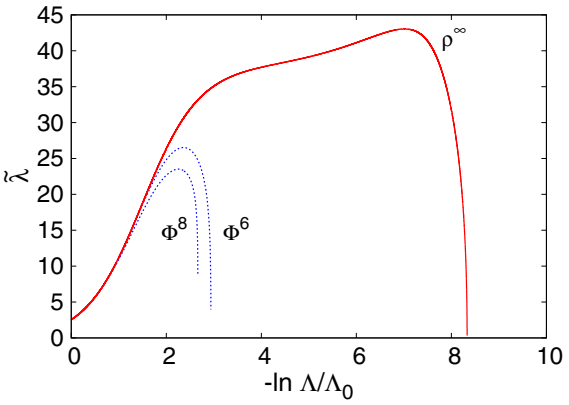

FIG. 5. (Color online) Flow of $\tilde{\lambda}$ at $T = 0.275J$ within different approximations. Shown are the results of a field expansion to order Φ^6 and Φ^8 (dashed blue lines) compared to the full dependence on ρ to first order in τ (red solid line).

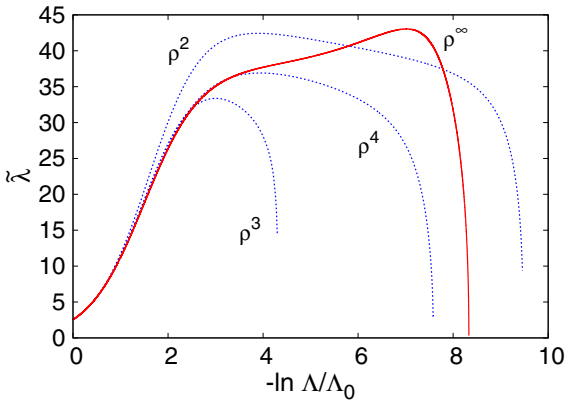

FIG. 7. (Color online) Flow of $\tilde{\lambda}$ at $T = 0.275J$ within an expansion in ρ to order ρ^2, ρ^3, and ρ^4 (dashed blue lines) compared to the full dependence on ρ (red solid line). All truncations keep only the first order in τ.

zero by a divergence of a higher-order vertex, much faster than in the approximation given by Eq. (3.3), where all powers of ρ are kept. The same behavior is also observed in the flow of $\tilde{\mu}$; see Fig. 6. In the Φ^8 approximation the suppression is even faster than in the Φ^6 truncation and what limits the flow is not the vanishing of the order parameter ρ^0 but the divergence of the higher-order vertices. This clearly shows that a fixed-order field expansion is not useful in this case. In Fig. 7 we show that, in contrast, the expansion on just the invariant ρ shows better convergence properties. The best alternative would be to directly explore the flow of $U_\Lambda(\rho,\tau)$ without any restrictions, which would, however, be numerically very costly. As we discuss now, the higher-order derivative terms are also important; one would thus have to analyze the full flow of $U_\Lambda(\rho,\tau)$ in conjunction with the full momentum dependence of the coupling functions $\mu_\Lambda(k)$, $\lambda_\Lambda(k)$, and $\Omega_\Lambda(k)$, or at least with including also higher-order derivative terms, which is numerically extremely challenging.

To gauge the importance of the k-dependent vertices, we finally compare the flow within an approximation where only the leading-order derivative terms present in Eq. (2.3) are kept with the approximation where the full momentum dependence of $\lambda_\Lambda(k)$, $\mu_\Lambda(k)$, and $\Omega_\Lambda(k)$ is included. In both approximations all local terms up to order Φ^6 or Φ^8 are included. As shown in Fig. 8, there are clear differences and the flow with the full momentum dependence is more stable. It thus seems that the higher-order derivative terms are non-negligible.

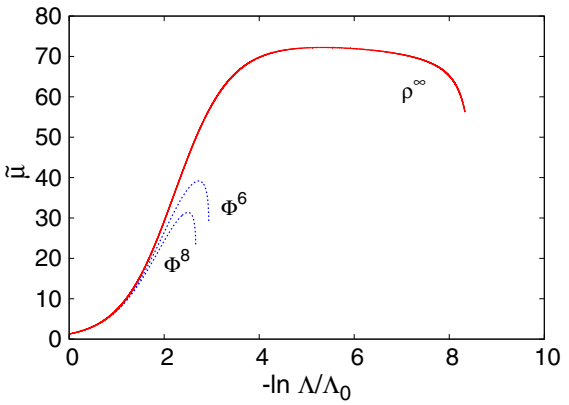

FIG. 6. (Color online) Flow of $\tilde{\mu}$ at $T = 0.275J$ within a field expansion to order Φ^6 and Φ^8 (dashed blue lines) compared to the full dependence on ρ to first order in τ (red solid line).

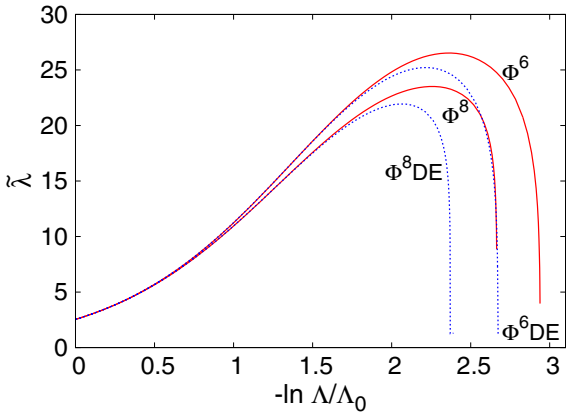

FIG. 8. (Color online) Flow of $\tilde{\lambda}$ at $T = 0.275J$ with (red solid lines) and without (dashed blue lines) higher-order derivative terms (see text; DE stands for first-order derivative expansion). Shown are results including all local terms up to order Φ^6 and to order Φ^8.

[1] L. Balents, Nature (London) **464**, 199 (2010).

[2] H. Kawamura and S. Miyashita, J. Phys. Soc. Jpn. **53**, 4138 (1984).

[3] J. V. José, L. P. Kadanoff, S. Kirkpatrick, and D. R. Nelson, Phys. Rev. B **16**, 1217 (1977).

[4] B. W. Southern and H.-J. Xu, Phys. Rev. B **52**, R3836 (1995).

[5] M. Wintel, H. U. Everts, and W. Apel, Phys. Rev. B **52**, 13480 (1995).

[6] H. Kawamura, A. Yamamoto, and T. Okubo, J. Phys. Soc. Jpn. **79**, 023701 (2010).

[7] L. Seabra, T. Momoi, P. Sindzingre, and N. Shannon, Phys. Rev. B **84**, 214418 (2011).

[8] M. V. Gvozdikova, P.-E. Melchy, and M. E. Zhitomirsky, J. Phys.: Condens. Matter **23**, 164209 (2011).

[9] P. Calabrese and P. Parruccini, Phys. Rev. B **64**, 184408 (2001).

[10] B. Delamotte, M. Dudka, Yu. Holovatch, and D. Mouhanna, Phys. Rev. B **82**, 104432 (2010).

[11] A. Olariu, P. Mendels, F. Bert, B. G. Ueland, P. Schiffer, R. F. Berger, and R. J. Cava, Phys. Rev. Lett. **97**, 167203 (2006).

[12] A. Yaouanc, P. Dalmas de Réotier, Y. Chapuis, C. Marin, G. Lapertot, A. Cervellino, and A. Amato, Phys. Rev. B **77**, 092403 (2008).

[13] H. Yamaguchi, S. Kimura, M. Hagiwara, Y. Nambu, S. Nakatsuji, Y. Maeno, and K. Kindo, Phys. Rev. B **78**, 180404(R) (2008).

[14] M. Schmidt, Z. Wang, Ch. Kant, F. Mayr, S. Toth, A. T. M. N. Islam, B. Lake, V. Tsurkan, A. Loidl, and J. Deisenhofer, Phys. Rev. B **87**, 224424 (2013); M. Hemmida, H.-A. Krug von Nidda, N. Büttgen, A. Loidl, L. K. Alexander, R. Nath, A. V. Mahajan, R. F. Berger, R. J. Cava, Yogesh Singh, and D. C. Johnston, *ibid.* **80**, 054406 (2009).

[15] M. Caffarel, P. Azaria, B. Delamotte, and D. Mouhanna, Phys. Rev. B **64**, 014412 (2001).

[16] B. Delamotte, D. Mouhanna, and M. Tissier, Phys. Rev. B **69**, 134413 (2004).

[17] H. Kawamura, J. Phys.: Condens. Matter **10**, 4707 (1998).

[18] B. W. Southern and A. P. Young, Phys. Rev. B **48**, 13170 (1993).

[19] N. Hasselmann, A. H. Castro Neto, and C. Morais Smith, Phys. Rev. B **69**, 014424 (2004); Europhys. Lett. **56**, 870 (2001).

[20] G. v. Gersdorff and C. Wetterich, Phys. Rev. B **64**, 054513 (2001).

[21] H. Kawamura, Phys. Rev. B **38**, 4916 (1988).

[22] M. Tissier, B. Delamotte, and D. Mouhanna, Phys. Rev. Lett. **84**, 5208 (2000).

[23] J. Berges, N. Tetradis, and C. Wetterich, Phys. Rep. **363**, 223 (2002).

[24] P. Kopietz, L. Bartosch, and F. Schütz, *Introduction to the Functional Renormalization Group* (Springer, Berlin, 2010).

[25] P. Azaria, B. Delamotte, and T. Jolicoeur, Phys. Rev. Lett. **64**, 3175 (1990).

[26] P. Azaria, B. Delamotte, F. Delduc, and T. Jolicoeur, Nucl. Phys. B **408**, 485 (1993).

[27] P. Azaria, B. Delamotte, T. Jolicoeur, and D. Mouhanna, Phys. Rev. B **45**, 12612 (1992).

[28] T. Dombre and N. Read, Phys. Rev. B **39**, 6797 (1989).

[29] C. Wetterich, Phys. Lett. B **301**, 90 (1993); T. R. Morris, Int. J. Mod. Phys. A **9**, 2411 (1994).

[30] N. Hasselmann, Phys. Rev. E **86**, 041118 (2012).

[31] N. Hasselmann and F. L. Braghin, Phys. Rev. E **83**, 031137 (2011); F. L. Braghin and N. Hasselmann, Phys. Rev. B **82**, 035407 (2010); K. Essafi, J.-P. Kownacki, and D. Mouhanna, Phys. Rev. E **89**, 042101 (2014); Phys. Rev. Lett. **106**, 128102 (2011).

[32] F. Benitez, J. P. Blaizot, H. Chaté, B. Delamotte, R. Méndez-Galain, and N. Wschebor, Phys. Rev. E **85**, 026707 (2012); **80**, 030103(R) (2009).

[33] M. Wintel, H. U. Everts, and W. Apel, Europhys. Lett. **25**, 711 (1994).